Microphase and Macrophase Separation in Multicomponent A/B/A−C Polymer Blends with Attractive and Repulsive Interactions

Megan L. Ruegg,[†] Benedict J. Reynolds,[†,‡] Min Y. Lin,[§,||] David J. Lohse,[§] and Nitash P. Balsara*[,†,⊥]

Department of Chemical Engineering, University of California, Berkeley, California 94720, Earth Science, Materials Sciences, and Environmental Energy Technologies Divisions, Lawrence Berkeley National Laboratory, University of California, Berkeley, California 94720, and ExxonMobil Research and Engineering, Annandale, New Jersey 08801

Received July 29, 2005; Revised Manuscript Received October 18, 2005

ABSTRACT: A balanced A−C diblock copolymer surfactant was used to organize mixtures of immiscible A and B homopolymers. The C block of the copolymer exhibits repulsive and attractive interactions with the A and B homopolymers, respectively, leading to rich phase behavior. Experimental results indicate the existence of a microphase-separated state at low temperatures, a homogeneous phase at intermediate temperatures, and macrophase separation at high temperatures. It is unusual for a microphase-separated blend to exhibit a homogeneous phase prior to macrophase separation. In this study, component A was saturated polybutadiene with 89% 1,2-addition, component B was polyisobutylene, block A of the diblock copolymer was chemically equivalent to component A, and block C of the diblock copolymer was saturated polybutadiene with 63% 1,2-addition. We use a combination of Flory−Huggins theory (FHT), self-consistent field theory (SCFT) and the random-phase approximation (RPA) to understand the origin of our observations. All of the parameters needed for the SCFT, FHT, and RPA calculations were obtained from independent measurements. The measured length scale of the periodic concentration fluctuations in the homogeneous state and the domain spacing of the microphase-separated blends were in close agreement with RPA and SCFT, respectively. The transition temperatures between phases predicted with theory were in reasonable agreement with the experimental measurements.

Introduction

Block and graft copolymers are often used to stabilize interfaces between immiscible polymers. Numerous fundamental studies have focused on the use of A−B diblock copolymers for organizing (or "compatibilizing") mixtures of A and B homopolymers.[1−31] In this case, there is no "affinity" or attractive interactions between the surfactant and the homopolymers; the A and B blocks exhibit athermal interactions with the A and B homopolymers, respectively. Interfacial activity is driven entirely by the repulsion between A and B chains. (We use A block to refer to an A chain that is part of a block copolymer and A to refer to an A homopolymer chain.) This approach has had limited success. Both experiments and theory show that symmetric A−B surfactants are effective at organizing critical blends of weakly segregated homopolymers, i.e., when the product $\chi_{AB}N$ is slightly greater than 2 (χ_{AB} is the Flory−Huggins interaction parameter for the A and B chains, and N is the number of repeat units per homopolymer chain).[1−3] There are, however, large regions of parameter space where A−B copolymers are not effective surfactants. For example, the addition of A−B diblock copolymers to blends for which $\chi_{AB}N$ is significantly greater than 2 leads to the formation of a third copolymer-rich phase, rather than adsorption of the block copolymer at the interface between the homopolymers.[4,21] There is thus a clear need for devising alternative strategies for designing polymeric surfactants.

One strategy is to use block copolymer surfactants that exhibit attractive interactions with one or both of the immiscible homopolymers.[32−41] In this article, we use an A−C diblock copolymer to organize A and B homopolymers. The C block is designed to have attractive interactions with the B homopolymer and repulsive interactions with the A homopolymer. This is analogous to surfactants for oil/water systems[42−47] wherein the hydrophilic portion of the surfactant exhibits attractive interactions with water and repulsive interactions with oil. In A/B/A−C mixtures, surfactant behavior is governed by both attractive and repulsive interactions. In polymeric systems, these interactions are quantified by three Flory−Huggins interaction parameters: χ_{AB}, χ_{BC}, and χ_{AC}. The availability of many parameters is not necessarily an advantage. A trial-and-error approach toward surfactant design, which has been reasonably effective in the case of A−B surfactants, is likely to fail in the A/B/A−C systems because of the vastness of the parameter space. It is therefore imperative that we understand the role of these parameters before they can be exploited in surfactant design strategies.

The random-phase approximation (RPA) has previously been used to describe the concentration fluctuations in homogeneous multicomponent polymer blends.[10,18,48,49] These fluctuations are described by a matrix of partial structure factors $\underline{S}(q)$ (q is the scattering vector) that describe correlations between different components in the system. Homogeneous systems have $\det[\underline{S}(q)] > 0$ for all values of q. The limit of stability of the homogeneous phase occurs when $\det[\underline{S}(q)] = 0$ at a particular value of $q = q^*$. The transition to macrophase separation is anticipated when $q^* = 0$, and the formation of periodic microphases is anticipated

* To whom correspondence should be addressed. E-mail: nbalsara@berkeley.edu.
† Department of Chemical Engineering, University of California.
‡ Earth Science Division, Lawrence Berkeley National Laboratory, University of California.
§ ExxonMobil Research and Engineering.
|| Present address: NIST Center for Neutron Research, National Institute of Standards and Technology, Gaithersburg, MD 20899.
⊥ Materials Sciences Division and Environmental Energy Technologies Division, Lawrence Berkeley National Laboratory, University of California, Berkeley.

10.1021/ma0516889 CCC: $33.50
Published on Web 01/14/2006

Table 1. Characterization of Polymers[a]

name	M_w (kg/mol)	PDI	ρ (g/mL)	percent 1,2-addition	n_D
hPB89(10)	10.1	1.01	0.8625	89.1	NA
dPB89(10)		1.01	0.9020	89.1	2.54
hPB89(24)	24.1	1.01	0.8636	90.4	NA
dPB89(24)		1.01	0.9070	90.4	2.79
hPB63(10)	9.9	1.02	0.8593	61.6	NA
dPB63(10)		1.02	0.9125	61.6	3.44
PIB(13)	12.5	1.04	0.9134	NA	NA
PIB(24)	24.0	1.05	0.9131	NA	NA
PIB(45)	44.6	1.04	0.9140	NA	NA
hPBPB(79−66)	78.5−65.4	1.01	0.8639	89.7−63.9	NA
dPBPB(79−66)		1.01	0.9122	89.7−63.9	3.10

[a] M_w is the weight-averaged molecular weight (the number of repeat units for deuterated polymers are equivalent to that of their hydrogenated counterparts), PDI is the polydispersity index, PDI $= M_w/M_n$, where M_n is the number-averaged molecular weight; ρ is the average density, and n_D is the number of deuterium atoms per C_4 repeat unit.

when $q^* > 0$. The phase behavior of mixtures beyond the stability limit can be obtained using Flory−Huggins theory (FHT) in the case of macrophase-separated systems or self-consistent field theory (SCFT) in the case of microphase-separated systems.

In this article, we have used small-angle neutron scattering (SANS) and light scattering to study the structure and phase behavior of A/B/A−C blends. The A and B homopolymers are weakly segregated ($\chi_{AB}N \approx 2$), and the molecular weight of the diblock copolymer, which is nearly symmetric, is roughly 6 times larger than that of the homopolymers. The weak segregation of the homopolymers is necessary in order to access the homogeneous phase. We study the properties of two multicomponent A/B/A−C blends that are microphase-separated at low temperatures, homogeneous at intermediate temperatures, and macrophase-separated at high temperatures. This nonmonotonic temperature dependence is due to the interplay between the attractive and repulsive interactions between the chains that comprise our system. We use SCFT to interpret the scattering profiles obtained in microphase-separated states and RPA to interpret the scattering profiles obtained in homogeneous states. To our knowledge, this combination of RPA and SCFT has not previously been used to study phase transitions in multicomponent polymer blends with both attractive and repulsive interactions. All of the SCFT and RPA calculations were completed with no adjustable parameters; the only inputs necessary were χ parameters and statistical segment lengths (l) determined from SANS experiments on homogeneous binary homopolymer mixtures. Thus, the agreement between theory and experiment is a reflection of a fundamental understanding of the phase behavior of these blends.

Experimental Methods

In the A/B/A−C polymer blends, component A was saturated polybutadiene with 89% 1,2-addition (sPB89), component B was polyisobutylene (PIB), and component C was saturated polybutadiene with 63% 1,2-addition (sPB63) (the prefix s stands for saturated and is replaced by h or d when we wish to specify whether the polymer is hydrogenated or deuterated, respectively). Our synthesis and characterization procedures are described in ref 34. Polybutadiene was synthesized via anionic polymerization. A diblock copolymer of polybutadiene, with a different percent 1,2-addition for each of the blocks (89% and 63%), was synthesized by sequential anionic polymerization. The C═C double bonds in the polybutadienes were saturated under high pressure using hydrogen or deuterium gas. Polyisobutylene was synthesized via cationic polymerization, also described in ref 34. The characteristics of the polymers used in this study are summarized in Table 1. The composition labels for our samples are based on our targets. Samples wherein the percentage of 1,2-addition deviated by more than 2% from the targets were discarded.

Binary and multicomponent blends were created via methods described in ref 34. The samples were pressed between two quartz disks and then annealed at 90 °C (unless otherwise specified) for 10 min to erase the effects of the shearing force applied to the sample during pressing. Our thermodynamic studies are focused on three blend systems labeled M00, M40, and M50. In each of the multicomponent blends, the volume fraction ratio of homopolymers A and B is held fixed at $\phi_A = 0.493$, which is the critical composition of the binary blend, according to Flory−Huggins theory. The volume fraction of the A−C block copolymer thus completely defines the blend composition. We refer to our blends as Mxy, where xy is the volume fraction of the block copolymer.

Small-angle neutron scattering (SANS) experiments were conducted on the NG7 beamline at the National Institute of Standards and Technology in Gaithersburg, MD. Raw data were converted to absolute coherent scattering intensity, I, as a function of q [$q = 4\pi\sin(\theta/2)/\lambda$, where θ is the scattering angle and λ is the wavelength of the incident beam), after corrections for detector sensitivity, background, empty cell, and incoherent scattering were made, using standard procedures.[50] For the deuterated components, corrections for the nonuniformity of deuterium labeling were made.[51] The upper limit of the SANS sample holder was 250 °C.

Small-angle light scattering (SALS) experiments were conducted with a 10-mW HeNe laser, with wavelength $\lambda_{light} = 633$ nm, directed through samples placed in a temperature-controlled heating unit. Scattered light was focused on a detector in the range of 4.33×10^{-4} nm$^{-1} < q < 1.85 \times 10^{-3}$ nm^{-1} using a beam stop and a focusing lens. (The definition of q given above holds for both light and neutron scattering.) Instrumental details are given in ref 52. The intensity was monitored as a function of time after the sample had been heated in a stepwise manner from one predetermined temperature to another. The upper temperature limit of the SALS sample holder was 250 °C.

Definitions. When discussing A/B/A−C ternary blends, the subscripts Ah and Bh refer to the A and B homopolymers, Ab and Cb refer to the A and C blocks of the copolymer, ACb refers to the entire block copolymer, and the subscripts A, B, and C refer to monomers of types A, B, and C, respectively. When discussing A/B, A/C, and B/C binary blends, we use the subscripts A, B, and C to refer to the both the homopolymers and the monomer types (leaving out the h for notational simplicity). We use a reference volume $v = 100$ Å^3, which is roughly the volume of a C_4 repeat unit of our components, as the basis for defining the following parameters: the Flory−Huggins interaction parameters χ_{mn} (m, n = A, B, C), the number of reference volume units per chain of each component (N_j), and the statistical segment lengths of the components (l_m), which describe the dependencies of the radius of gyration, $R_{g,m}$, on N_m ($R_{g,m} = N_m l_m^2/6$). Because the polymer density is temperature-dependent, N_j is also temperature-dependent. N_j of deuterated components are equal to that of their hydrogenated counterparts. All definitions and equations are described fully in ref 34.

Theory. We make extensive use of three well-known theoretical frameworks to analyze our data: the random-phase approximation (RPA), which applies to homogeneous blends; Flory−Huggins theory (FHT), which is appropriate for studying systems that undergo macrophase separation; and self-consistent field theory (SCFT), which is particularly well-suited for studying microphase-separated systems. The procedure that we adopt in this article is identical to that used in our previous publication.[34] We therefore present a very brief summary of our methodology here.

Random-Phase Approximation for Homogeneous Blends. The coherent scattering profile from an A/B/A−C multicomponent blend is given by[53−55]

$$I(q) = \mathbf{B}^T \underline{\underline{S}}(q) \mathbf{B} \tag{1}$$

where **B** is a column-vector describing the contrast and $\underline{\underline{S}}(q)$ is the

Table 2. Compositions of Binary Blends Used to Measure χ

				component		
blend	A	B	C	ϕ_A	ϕ_B	ϕ_C
B1	dPB89(10)	PIB(45)	−	0.673	0.327	−
B2	hPB89(10)	−	dPB63(10)	0.493	−	0.507
B3	−	PIB(13)	dPB63(10)	−	0.477	0.523

3×3 structure factor matrix. The elements of **B** are related to the scattering length density of each component j [$B_j = (b_j - b_{Bh})/v$, where j=Ah, Ab, Cb and b_j is the scattering length of a reference volume unit]. Because of incompressibility, the correlations with the background component are eliminated, as long as the background component is not connected to any of the other components (in our case, the background component is chosen to be the B homopolymer). The elements of the structure factor matrix are a function of N_j, ϕ_j, ν_j, and l_j for each component, as well as the three binary interaction parameters (χ_{mn}, where m, n = A, B, C) in this system and the scattering vector, q. The details of the RPA for homogeneous multicomponent blends are given in Appendix A of ref 34. For binary homopolymer blends, eq 1 reduces to the well-known result

$$I(q) = \frac{(b_A - b_B)^2}{v}\left[\frac{1}{N_A\phi_A P_A(q)} + \frac{1}{N_B\phi_B P_B(q)} - 2\chi_{AB}\right]^{-1} \quad (2)$$

where the Debye function, $P_m(q)$, is, by definition

$$P_m(q) = \frac{2}{x_m^2}[\exp(-x_m) + x_m - 1] \qquad (m = \text{A, B, C})$$

with $x_m = q^2R_{g,m}^2 = q^2N_m l_m^2/6$.

Flory−Huggins Theory and Self-Consistent Field Theory. The Flory−Huggins expression for the Helmholtz free energy per unit volume, f, of a structureless homogeneous A/B/A−C mixture is

$$\frac{fv}{kT} = \sum_i \frac{\phi_i}{N_i}\ln\phi_i + \frac{1}{2}\sum_{m,n}\chi_{mn}\phi_m\phi_n - \frac{1}{2}\sum_{i,m,n}\frac{\chi_{mn}\phi_{i,m}\phi_{i,n}}{\phi_i} \quad (3)$$

where i = (Ah, Bh, ACb); ϕ_{Ah}, ϕ_{Bh}, and ϕ_{ACb} are the average volume fractions of the A homopolymer, B homopolymer, and A−C diblock copolymer, respectively; and N_{Ah}, N_{Bh}, and N_{ACb} are the number of reference volume units in the three species. The subscripts m and n represent the set (A, B, C), where ϕ_A, ϕ_B, and ϕ_C are the average volume fractions of monomers of type A, B, and C, respectively, and χ_{AB}, χ_{AC}, and χ_{BC} are the three interaction parameters. The notation $\phi_{i,m}$ is used to represent the volume fraction of monomer of type m from species of type i, where m = (A, B, C) and i = (Ah, Bh, ACb), i.e., $\phi_A = \phi_{Ah,A} + \phi_{Bh,A} + \phi_{ACb,A} = \phi_{Ah} + \phi_{Ab}$. The reference state, implicit in this expression for the free energy, is that of each species forming a pure structureless phase.

Periodic structures are described using self-consistent field theory (Appendix B of ref 34).[56−58] In these phases, the volume fractions of the components, $\phi_{i,m}$, are periodic functions of position. We use $\phi_{i,m}(z)$ to describe these functions and the term $\phi_{i,m}$ to refer to the average value of $\phi_{i,m}(z)$. The parameter z is a Cartesian one-dimensional coordinate made dimensionless using $v^{1/3}$. By assuming that our concentration profiles vary only in one linear dimension, we restrict ourselves to lamellar periodic structures. Self-consistent field theory substitutes interactions between the polymers with equivalent external fields. Given these external fields, the volume fraction profiles, $\phi_{i,m}(z)$, are found that minimize the free energy. Self-consistency then requires that the external fields, produced by the volume fraction profiles, must be consistent with the external fields originally proposed. In this work, SCFT is used to calculate the volume fraction profiles, $\phi_{i,m}(z)$, and free energy densities, f, of ordered structures. A detailed description of the method is given in refs 56−58. The procedure employed in this work is described in Appendix B of ref 34. Other authors have conducted SCFT calculations for multicomponent blends of immiscible A and B homopolymers and an A−B diblock copolymer.[59,60]

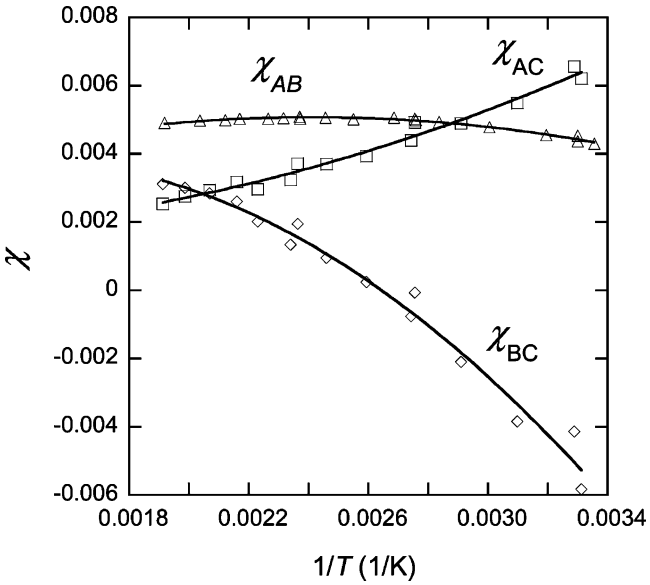

Figure 1. χ parameters obtained for the three binary blends A/B (△), A/C (□), and B/C (◇) from RPA fits. Typical values of the error on measuring χ parameters are 5−10%.

Our SCFT calculations are limited in scope because they are restricted to one dimension, and we neglect the effect of concentration fluctuations. Our calculations thus do not distinguish between complex periodic phases such as spherical or bicontinuous microemulsion and lamellar phases (other authors have used a Monte Carlo approach to study the transition from a lamellar phase to a bicontinuous microemulsion[61]).

Results and Discussion

Binary χ Parameters and Statistical Segment Lengths. The SANS profiles were measured for three binary blends, A/B, A/C, and B/C (blends B1, B2, and B3, respectively, described in Table 2), at a variety of temperatures. The values of χ_{mn} and l_m in the RPA (eq 2) were fit simultaneously to the three sets of data at these temperatures, thereby ensuring that the statistical segment lengths for each polymer obtained from different blends were identical (i.e., the l_A values for polymer A in the A/B blend and in the A/C blend are constrained to be the same). We can define a parameter $l_{mon,m} = l_m\sqrt{v_{mon,m}/v}$, where $v_{mon,m}$ is the monomer volume based on a C_4 repeat unit. This parameter ($l_{mon,m}$) is the statistical segment length based on the C_4 repeat-unit volume. The two statistical segment lengths are related as follows: $N_m l_m^2 = N_{mon,m} l_{mon,m}^2$ (where $N_{mon,m}$ is the number of C_4 repeat units per chain.) It was determined that the values of $l_{mon,m}$ for these polymers are temperature-independent: $l_{mon,A} = 0.60$ nm, $l_{mon,B} = 0.55$ nm, and $l_{mon,C} = 0.71$ nm. The theory was refit to the data using the predetermined values of $l_{mon,m}$, and thus, the only adjustable parameters were the χ_{mn} values. The binary blends used to obtain χ in this study are identical to those used in ref 34 except for the fact that the temperature range covered in this study is larger. The current χ parameters and those determined previously[34] are shown in Figure 1. A least-squares quadratic fit through each data set (including the data from ref 34 and the most recent data) is used to determine the temperature dependence of the χ parameters. We thus obtain

$$\chi_{AB} = 0.00034 + 3.94\frac{1}{T} - 817\frac{1}{T^2} \quad (4)$$

$$\chi_{AC} = 0.00209 - 1.18\frac{1}{T} + 747\frac{1}{T^2} \quad (5)$$

$$\chi_{BC} = -0.00085 + 6.87\frac{1}{T} - 2480\frac{1}{T^2} \quad (6)$$

Furthermore, the values of $l_{mon,m}$ are taken as the averages of the present fits and those given in ref 34: $l_{mon,A} = 0.55$ nm, $l_{mon,B} = 0.58$ nm, and $l_{mon,C} = 0.75$ nm. We will use these average χ and $l_{mon,m}$ values from this point forward.

Phase Behavior of an A/B Binary Blend (M00). The A/B binary blend that forms the basis of our work on multicomponent A/B/A−C blends is labeled M00 in Table 3. It is a blend of dPB89(24) and PIB(24) with $\phi_A = 0.493$, which is the critical composition for the blend calculated using Flory−Huggins theory. The A/B blend was prepared at 35 °C, transported to NIST at room temperature, and examined by SANS. The SANS results from M00 are summarized in Figure 2. The blend was initially cooled to −9 °C and studied as a function of increasing temperature. The SANS profile expected from a homogeneous blend is well-established.[55] At high q, $I(q) \sim q^{-2}$, and the slope dI/dq decreases monotonically with decreasing q, reaching a plateau as q approaches 0 $\{I(q \rightarrow 0) \sim [1/(N_A\phi_A) + 1/(N_B\phi_B) - 2\chi_{AB}]^{-1}\}$. The SANS profile from our A/B blend at −9 °C is not consistent with this expectation. At high q, the −9 °C scattering profile does not follow the scaling $I(q) \sim q^{-2}$. Furthermore, dI/dq increases monotonically with decreasing q. The scattering profile at low q ($q < 0.025$ nm^{-1}) exhibits Porod scattering ($I \sim q^{-4}$) instead of a plateau, indicating the presence of highly phase-separated domains with narrow interfaces. As the temperature was increased, the high-q scattering intensity increased significantly, and the low-q scattering decreased. The scattering profile obtained at 25 °C, which shows the standard signatures of scattering from homogeneous blends including a low-q plateau and $I(q) \sim q^{-2}$ at high q, dramatically differs from that obtained at the lower temperatures (Figure 2). The RPA (eq 2) was used to fit this profile with χ_{AB} as the only adjustable parameter (the values of l_A and l_B were previously determined from homogeneous binary blends). The solid curve in the inset of Figure 2 is the result of this fitting, which gives $\chi_{AB} = 0.0044$. This value is identical to that obtained from the blend B1 (eq 4). It is thus clear that our A/B blend is homogeneous at 25 °C. Increasing the sample temperature to 27 °C leads to a SANS profile with a peak at $q = 0.0173$ nm^{-1}. The presence of a scattering peak, which is not consistent with the RPA-based $I(q)$ profile for homogeneous binary blends, indicates that our blend is undergoing spinodal decomposition.[62] The scattering peak is seen up to 35 °C (Figure 2). Increasing the sample temperature further to 40 °C leads to a macrophase-separated sample, i.e., a SANS profile that is qualitatively similar to that obtained at −9 °C.

The above discussion establishes that the M00 blend is near the critical point at room temperature. Although we have clearly established that this blend is phase-separated at temperatures >25 °C and homogeneous at 25 °C, the state of the blend at temperatures <25 °C remains to be established. The data in Figure 1 indicate that χ_{AB} decreases with decreasing temperature in the 20−40 °C window. This implies that the blend should become increasingly homogeneous with decreasing temperature. Our inability to homogenize M00 at 20 °C might be due to nonequilibrium effects; it is thus conceivable that very long equilibration times at 20 °C might have led to observations of a homogeneous sample. We were unable to perform such experiments because of limited access to the SANS instrument.

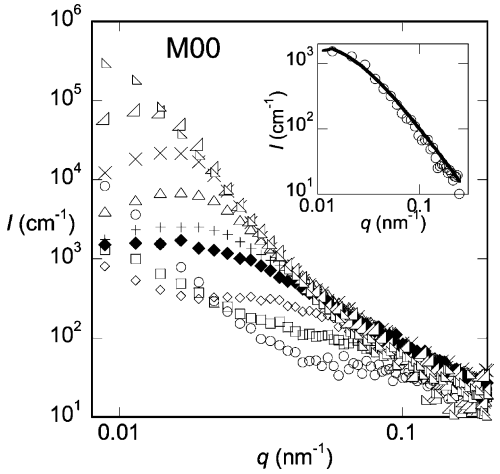

Figure 2. SANS data obtained from blend M00. I vs q is plotted at selected temperatures: −9 (○), 10 (□), 20 (◇), 25 (◆), 27 (+), 29 (△), 31 (×), 35 (right triangle pointing left), and 40 (right triangle pointing right) °C. Inset: SANS data obtained from blend M00 at 25 °C. The solid curve is the result of fitting the RPA, as described in the text.

Table 3. Compositions of Blends Used in Surfactancy Study

				component		
blend	A	B	A−C	ϕ_A	ϕ_B	ϕ_{A-C}
M00	dPB89(24)	PIB(24)	−	0.493	0.508	0.000
M40	dPB89(24)	PIB(24)	hPBPB(79−66)	0.296	0.305	0.400
M50	dPB89(24)	PIB(24)	hPBPB(79−66)	0.246	0.254	0.500
M50b	hPB89(24)	PIB(24)	dPBPB(79−66)	0.246	0.254	0.500

Additionally, we conducted neutron scattering experiments on blend B1 at low temperatures (down to −9 °C). We did not see an upturn in χ_{AB} at low temperatures as would be suggested by the phase separation observed in blend M00 at −9 °C. However, a small change in χ_{AB} would be more difficult to detect in a blend that is far from the critical point, such as in blend B1. Blend M00 is much closer to the critical point at −9 °C. Our limited understanding of the A/B blend does not affect the present study because the multicomponent A/B/A−C blends were studied at temperatures between 30 and 199 °C. It is clear that the A/B blend is phase-separated in this temperature window. In a symmetric blend ($N = N_A = N_B$), $\chi_{AB}N = 2$ at the critical point. In an asymmetric blend, $\chi_{AB}N_{avg} = 2$ at the critical point, where N_{avg} is defined by

$$\chi_c = 2\left[\frac{1}{2(N_A)^{1/2}} + \frac{1}{2(N_B)^{1/2}}\right]^2 = \frac{2}{N_{avg}} \quad (7)$$

For blend M00, the calculated value of $\chi_{AB}N_{avg}$, based on eqs 4 and 7, ranges from 2 to 2.6 in the 30−199 °C temperature window. The SANS data from samples B1 and M00 are entirely consistent in this temperature window. We also conducted light scattering experiments on sample M00 but were unable to distinguish between critical opalescence and phase separation. The sample had a cloudy appearance at all temperatures.

It is worth noting that designing and characterizing a weakly segregated A/B blend was nontrivial because the interaction parameter is nearly independent of temperature (Figure 1). It is, however, a convenient model system for studying surfactancy because the temperature-dependent effects that we observe in the multicomponent A/B/A−C blends can be attributed entirely to changes in the interactions between the surfactant and the coexisting phases.

Scattering from Multicomponent Blends. Multicomponent RPA calculations provide a glimpse of the rich phase behavior

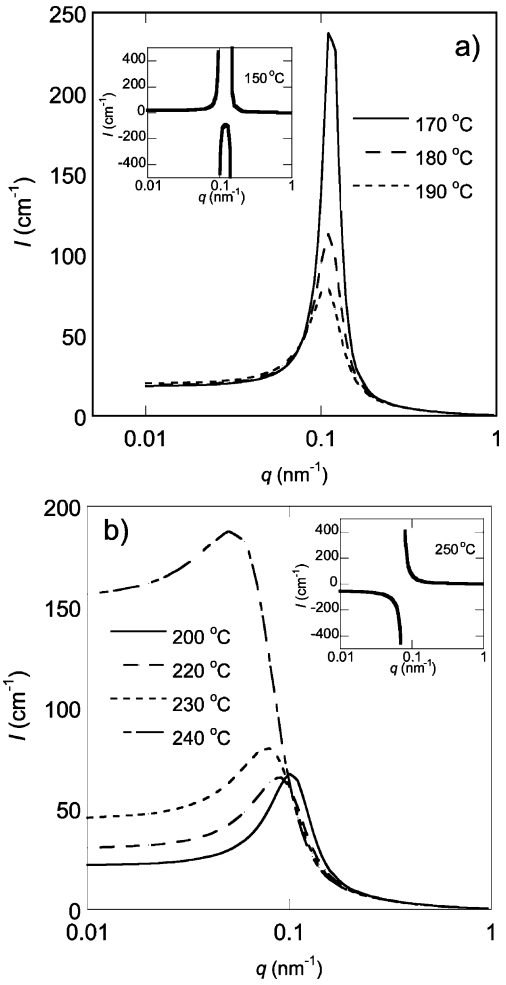

Figure 3. RPA predictions for the SANS profiles, I vs q, in the homogeneous phase for blend M40 at (a) 170−190 and (b) 200−240 °C. The inset in part a is the RPA prediction for blend M40 at 150 °C showing the signature of microphase separation, and the inset in part b is the RPA prediction for blend M40 at 250 °C showing the signature of macrophase separation.

expected in A/B/A−C blends, because of the presence of both attractive and repulsive interactions in our system. RPA-based scattering profiles reflect the nature of concentration fluctuations in homogeneous blends, which, in turn, are announcements of impending phase transitions. In Figure 3a, we show the scattering intensity profile of blend M40 in the 170−190 °C range calculated using RPA. The scattering profiles of blends M40 and M50 are dominated by the contrast between the deuterium-labeled dPB89 chains and the other components, which are hydrogenated polyolefins. Whereas the contrast between the blocks of the hPBPB(79−66) diblock copolymer is negligible, there is substantial contrast between PIB and the hPBPB(79−66) diblock copolymer because of density differences (Table 1). All of these scattering length density differences are taken into account in our multicomponent RPA calculations. The RPA calculations indicate the presence of a sharp peak in $I(q)$ at $q \approx 0.11$ nm^{-1} that decreases in intensity as temperature increases (Figure 3a). The RPA profile of M40 at 150 °C, shown in the inset of Figure 3a, contains two poles. This is a standard signature of microphase separation. The RPA thus predicts the formation of periodic microphases at temperatures ≤150 °C. In Figure 3b, we show the RPA predictions for $I(q)$ at temperatures between 200 and 240 °C. In this temperature range, the low-q scattering intensity ($q < 0.03$) increases with increasing temperature. The pronounced scattering peak seen

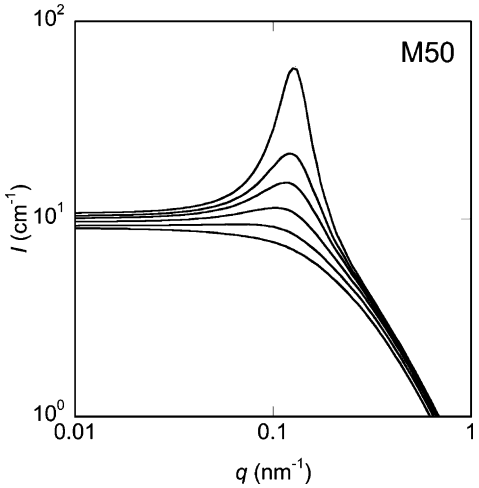

Figure 4. RPA predictions for the SANS profiles, I vs q, in the homogeneous phase for blend M50 at 150, 170, 190, 230, 300, and 400 °C (in order of decreasing peak intensity).

at lower temperatures (below 200 °C) is reduced to a weak shoulder at 240 °C. The scattering profile computed at 250 °C contains a single singularity, as shown in the inset of Figure 3b. This is a standard signature of a macrophase separation transition.

In Figure 4, we show $I(q)$ calculated using eq 1 for blend M50 at temperatures between 150 and 400 °C (the upper temperatures are not experimentally accessible). We find a sharp peak in $I(q)$ at $q \approx 0.10-0.13$ nm^{-1} that decreases in intensity as temperature increases. At temperatures ≤131 °C, RPA predicts the formation of periodic microphases (same signature as the inset of Figure 3a; not shown for brevity). The low-temperature behaviors obtained from M50 and M40 are similar except for the difference in the numerical value of the microphase separation transition temperature. At high temperatures, however, the RPA predictions for M40 and M50 are qualitatively different (compare Figures 3b and 4). As temperature increases, the scattering intensity from M50 decreases monotonically at all q values (Figure 4). Sample M50 is thus predicted by RPA to be single-phase at all temperatures above 131 °C.

The measured SANS data obtained from blend M40 at selected temperatures are shown in Figure 5. The scattering intensities have been multiplied by factors of 10 to delineate the data sets. The sample exhibits a well-defined scattering peak at temperatures ≤169 °C that decreases in intensity as the temperature is increased. At 189 °C, a large increase in low-q scattering indicates the onset of macrophase separation. The measured SANS profiles obtained from sample M50, shown in Figure 6, are qualitatively similar to those obtained from M40. (The scattering intensities have been multiplied by factors of 10 to delineate the data sets.) Well-defined scattering peaks were obtained between 30 and 189 °C, and clear signatures of macrophase separation were observed at temperatures ≥199 °C.

It is clear from the SANS experiments that both M40 and M50 exhibit macrophase separation at elevated temperatures: ≥189 °C in the case of M40 and ≥199 °C in the case of M50. This is in partial agreement with the RPA predictions wherein macrophase separation at elevated temperatures is predicted only in the case of M40. In addition, the RPA prediction of the macrophase separation temperature of 245 °C is well above that seen experimentally for blend M40. Of course, the RPA calculations indicate only the limit of stability of the homogeneous phase. A more complete analysis is required to determine

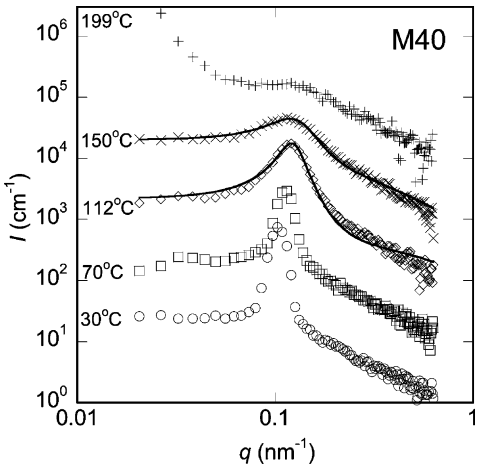

Figure 5. SANS profiles, I vs q, obtained from blend M40 at selected temperatures: 30 (○), 70 (□), 112 (◇), 150 (×), and 199 (+) °C. The scattering intensities have been multiplied by the following factors to delineate the data sets: 10 (70 °C), 10^2 (112 °C), 10^3 (150 °C), and 10^4 (199 °C). The solid curves at 112 and 150 °C are the Teubner−Strey scattering profile fits to the data.

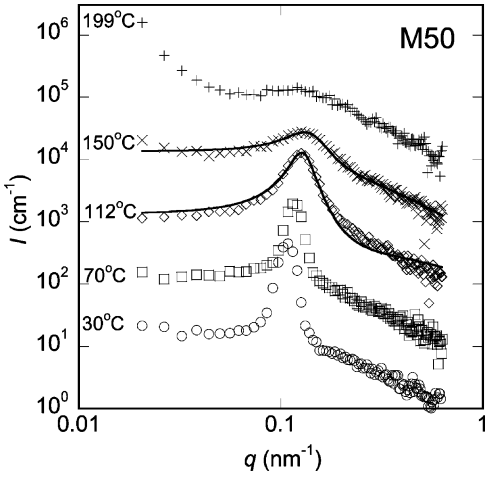

Figure 6. SANS profiles, I vs q, obtained from blend M50 at selected temperatures: 30 (○), 70 (□), 112 (◇), 150 (×), and 199 (+) °C. The scattering intensities have been multiplied by the following factors to delineate the data sets: 10 (70 °C), 10^2 (112 °C), 10^3 (150 °C), and 10^4 (199 °C). The solid curves at 112 and 150 °C are the Teubner−Strey scattering profile fits to the data.

the limit of metastability of the homogeneous phase in our A/B/A−C mixtures. This analysis will be presented shortly.

Our detailed thermodynamic analysis begins with an examination of the scattering peaks that are obtained in M40 and M50 over a wide temperature window. These peaks could, in principle, indicate the formation of ordered microphases such as lamellae, disordered microphases such as microemulsions, or homogeneous phases such as those described by RPA (Figures 3 and 4). We have added a nearly symmetric A−C block copolymer to a 50/50 blend of A and B homopolymers. We thus expect the ordered phase to have a lamellar morphology. In previous work, we have relied on the Teubner−Strey analysis to distinguish between lamellar phases and microemulsions.[34] The scattering profile from microemulsions, according to the Teubner−Strey (T−S) analysis, is given by

$$I(q) = \frac{1}{a + bq^2 + cq^4} + I_{\mathrm{bgd}}(q) \tag{8}$$

where a, b, and c are fitting parameters. We use $I_{\mathrm{bgd}}(q)$ to account for the fact the T−S equation was developed for oil/water microemulsions and, thus, does not account for scattering contributions due to the connectivity of polymer chains. $I_{\mathrm{bgd}}(q)$ is assumed to be of the form $I_{\mathrm{bgd}}(q) = (eq^2 + f)^{-1}$, where e and f are fitting constants. We do not have rigorous justification for the proposed splitting of $I(q)$. The solid curves in Figures 5 and 6 are the least-squares fits of eq 8 through the data with a, b, c, e, and f as adjustable constants. The values of the constants thus obtained are given in Table 4 for all data sets. They enable determination of the domain spacing, d, and correlation length, ξ, given by

$$\xi = \left[\frac{1}{2}\left(\frac{a}{c}\right)^{1/2} + \frac{1}{4}\frac{b}{c}\right]^{-1/2} \tag{9}$$

$$d = 2\pi\left[\frac{1}{2}\left(\frac{a}{c}\right)^{1/2} - \frac{1}{4}\frac{b}{c}\right]^{-1/2} \tag{10}$$

The values of ξ and d thus obtained are also included in Table 4.

Table 4. Teubner−Strey Fitting Parameters

blend	T (°C)	a (cm)	b (cm nm^2)	c (cm nm^4)	d (nm)	ξ (nm)
M40	90	0.1501	−21.13	775.35	53.54	83.77
M40	112	0.0571	−7.02	239.88	51.26	49.97
M40	131	0.0715	−7.74	261.03	50.17	34.05
M40	150	0.0843	−8.06	281.42	49.97	25.89
M40	169	0.0831	−6.36	246.03	50.22	19.15
M50	90	0.3075	−40.38	1367.50	51.51	93.22
M50	112	0.0994	−11.36	352.77	49.00	53.97
M50	131	0.1364	−13.83	413.56	47.57	37.29
M50	150	0.1671	−14.04	407.02	45.88	25.75
M50	169	0.1974	−14.82	440.92	45.60	21.45
M50	189	0.2704	−18.07	596.22	46.55	18.04

For sample M40, the T−S analysis was applicable at temperatures between 90 and 169 °C. At temperatures below 90 °C (e.g., T = 70 °C in Figure 5), the scattering peak was much narrower than predicted by the T−S analysis, regardless of the values of a, b, and c. Following previous work,[34] we conclude that we have a lamellar phase in M40 at temperatures below 90 °C.

At temperatures between 90 and 169 °C, the T−S parameters are qualitatively similar (Table 4). In particular, the fitting parameter b is negative in this temperature window. In the case of oil/water/surfactant mixtures, a negative value of b is taken as an indication of the presence of interfaces, whereas a positive value of b indicates the formation of a homogeneous phase with periodic concentration fluctuations. Whether this conclusion is applicable to polymer-in-polymer microemulsions will be addressed shortly.

The T−S analysis for sample M50 gives results that are very similar to those described above for M40, as can be seen in Table 4. We conclude that M50 forms a lamellar phase at temperatures below 90 °C, and the T−S analysis, which is valid at temperatures between 90 and 189 °C, gives negative values of b throughout our temperature window.

The periodic length scale d obtained from the T−S analysis is a weak function of temperature for both M40 and M50. As shown in Table 4, d varies between 45 and 54 nm, regardless of blend composition and temperature. However, the correlation length, ξ, increases rapidly with decreasing temperature. As shown in Table 4, ξ of M50 increases from 18 to 93 nm when the temperature decreases from 189 to 90 °C, and ξ of M40 increases from 19 to 84 nm when the temperature decreases from 169 to 90 °C. This rapid increase in correlation length appears to be a signature of the transition from a microemulsion to a lamellar phase in the A/B/A−C mixtures.

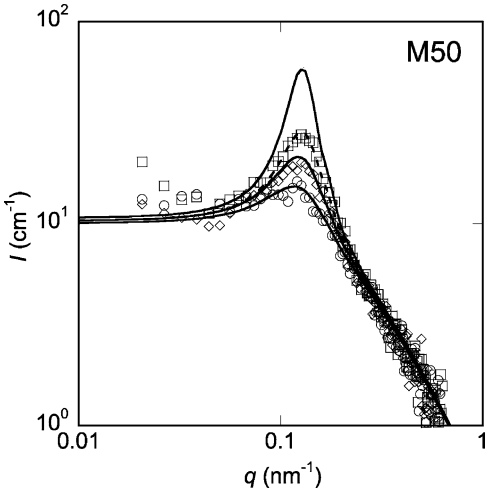

Figure 7. RPA predictions (solid curves) and SANS profiles (open circles) for blend M50 at 150 (□), 169 (◇), and 189 (○) °C. The dotted curve corresponds to adjusting a χ parameter such that the theory matches the data (see text).

In our previous work,[34] we were able to substantiate our conclusion regarding the presence of lamellar phases by performing experiments on A/B/A−C blends in which the A−C block copolymer was labeled with deuterium (instead of the A homopolymer). We conducted similar experiments on M50b (see Table 3 for composition) but were unable to find the same signatures reported in ref 34.[63] This is entirely due to differences in the self-assembly characteristics of the present samples and those studied in ref 34.

We now return to an interpretation of the scattering peaks observed from disordered M40 and M50 samples. Figure 7 shows the RPA prediction (solid curves) and SANS data (open symbols) for blend M50 at temperatures between 150 and 189 °C. The RPA theory accurately captures the low-q plateau of $I = 10$ cm^{-1}, the location of the scattering peak at $q \approx 0.12$ nm^{-1}, and the $I \sim q^{-2}$ tail at high q for all three temperatures. The theory also captures the peak intensity at 169 and 189 °C, but overpredicts the peak intensity at 150 °C. The agreement between theory and experiment in Figure 7 is remarkable considering that all of the 10 parameters needed for the RPA calculations (three χ parameters, three statistical segment lengths, and four chain lengths) were obtained from independent experiments. There are slight differences between theory and experiment at 150 °C. If we hold two of the three χ parameters constant and change the third, the theory exactly overlaps the SANS data. For example, if we hold χ_{AC} and χ_{BC} constant, the value of χ_{AB} required to fit the data is 0.0049. The result of this fit is shown as the dotted line in Figure 7. Similarly, if we hold χ_{AB} and χ_{BC} constant, the value of χ_{AC} required to fit the data is 0.0032, and if we hold χ_{AB} and χ_{AC} constant, the value of χ_{BC} required to fit the data is 0.0020. The curves resulting from the second two fits are not shown in Figure 7, as they are almost identical to the dotted line shown for the first fit. The values of the χ parameters determined from binary homogeneous blends at 150 °C were 0.0051, 0.0035, and 0.0015 for χ_{AB}, χ_{AC}, and χ_{BC}, respectively. Thus, the results of changing one of the χ parameters to fit the data at 150 °C is within the error of measuring χ from binary homogeneous blends. We take the quantitative agreement between RPA and the measured SANS profiles as an indication that M50 is homogeneous at temperatures between 150 and 189 °C. A similar analysis conducted on sample M40 indicated that this blend was homogeneous at 169 °C. The results were very similar to those shown in Figure 7 and are thus omitted for brevity.

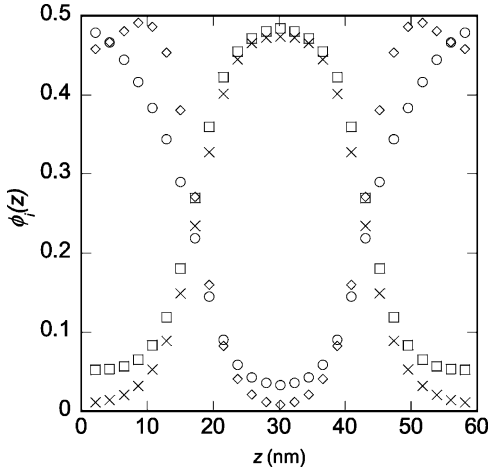

Figure 8. Equilibrium volume fraction profiles for blend M50 at 30 °C ($d = 60$ nm) predicted by SCFT. The volume fraction of each component is plotted vs distance: homopolymer A (○), homopolymer B (□), block A of the A−C diblock copolymer (◇), and block C of the A−C diblock copolymer (×).

The windows of microphase separation for samples M40 and M50 are thus 30−160 and 30−140 °C, respectively. We use SCFT to analyze the SANS data in this regime. The SCFT prediction for the domain spacing of blend M50 at 30 °C was 59 nm (based on an examination of the minimum free energy as a function of domain spacing). Typical equilibrium concentration profiles obtained from these calculations are given in Figure 8 where the z dependence of the periodic component volume fractions $\phi_{i,m}(z)$ for M50 at 30 °C are shown for a d spacing of 60 nm, which is slightly different from the predicted equilibrium spacing of 59 nm because of discretization limitations. As expected, the homopolymer volume fraction profiles are periodic, and the A block penetrates the A-homopolymer-rich phase while the C block penetrates the B-homopolymer-rich phase. The A block is drawn toward the interface, resulting in peaks in $\phi_{AB}(z)$ at $z = 9$ and 51 nm. No such peak is seen in $\phi_{Cb}(z)$ because the C block stretches away from the interface due to the attractive interactions between the B homopolymer and the C block. Similar SCFT calculations enabled determination of d_{SCFT} of M50 at temperatures up to 130 °C. Above this temperature, we found that the SCFT calculations did not converge on profiles that were consistent with the imposed constraints.

In Figure 9, we compare the experimentally determined values of the periodicity, d_{expt}, for M50 ($d_{expt} = 2\pi/q_{SANS\ peak}$, where $q_{SANS\ peak}$ is the location of the SANS peak) with theoretical predictions. The d_{expt} values exhibit a nonmonotonic temperature dependence, first decreasing with increasing temperature and then increasing with increasing temperature. The dashed curve represents d_{SCFT}, and the solid curve represents the RPA-based predictions ($d_{RPA} = 2\pi/q_{RPA\ peak}$, where $q_{RPA\ peak}$ is the location of the RPA peak). We find excellent agreement between theory and experiment over the entire temperature window. The difference between the theoretical and experimental d values is less than 1 nm at most temperatures. The maximum deviation between theory and experiment is seen at 190 °C, where we see a difference of 3.4 nm. The vertical lines in Figure 9 show the location of the phase boundaries (the line for the lamellar-to-microemulsion transition was based on SANS and T−S, the line for the microphase-separated-to-homogeneous transition was based on agreement between SANS and RPA, and the line for the homogeneous-to-macrophase-separated transition was based on SANS). It is evident that all aspects of microphase separation and the homogeneous state in M50 in the 30−190 °C temper-

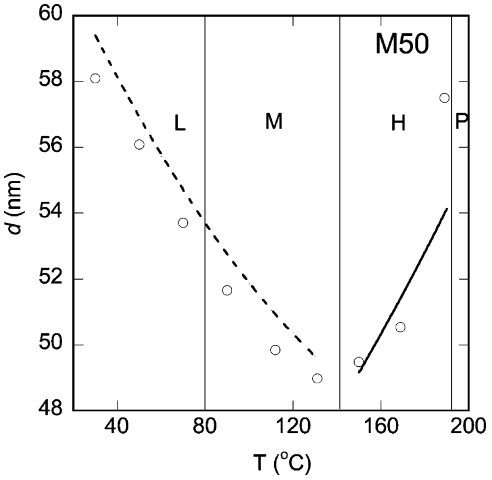

Figure 9. Domain spacing as a function of temperature for blend M50 as determined by SANS (○) and predicted by SCFT (dotted curve) or RPA (solid line). The solid vertical lines indicate phase transitions (L is a lamellar phase, M is a microemulsion, H is a homogeneous phase, and P is macrophase-separated phase).

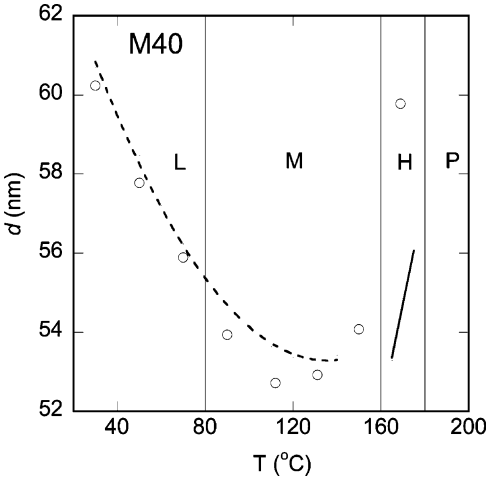

Figure 10. Domain spacing as a function of temperature for blend M40 as determined by SANS (○) and predicted by SCFT (dotted curve) or RPA (solid line). The solid vertical lines indicate phase transitions (L is a lamellear phase, M is a microemulsion, H is a homogeneous phase, and P is a macrophase-separated phase).

ature window are accurately captured by the combination of SCFT and RPA. Our simple SCFT analysis correctly predicts the experimental *d* spacing obtained from lamellar and microemulsion phases but does not distinguish between these two possibilities. In principle, the SCFT calculations should be able to predict phase behavior at all locations where the RPA is not valid. This is because both theories are mean-field approximations. In contrast, we see a small but finite gap between our SCFT and RPA calculations in Figure 9. Whether this is due to the limited dimensionality of the phases that have been studied by SCFT or limitations arising from the numerical nature of the calculations (finite box size, discretization, etc.) remains to be established. It is also conceivable that the microphase-to-homogeneous phase transition is a second-order phase transition. In this case, numerical mean-field techniques would break down because of the increasing importance of fluctuation corrections.[64−66] Despite these limitations, the quantitative correspondence between experiment, SCFT predictions, and RPA calculations shown in Figure 9 has, to our knowledge, not been demonstrated in prior work.

The SCFT/RPA analysis was repeated for sample M40, and the temperature dependence of the *d* spacing obtained by theory and experiment is shown in Figure 10. Again, we see quantitative agreement between theory and experiment in the entire temperature window.

Finally, we discuss the macrophase separation transition seen in both M40 and M50 as a function of increasing temperature. Our SANS measurements indicate that this transition occurs at 179 ± 10 °C in M40 and 194 ± 5 °C in M50. These conclusions were confirmed by SALS. In Figure 11, we show the temperature dependence of the SALS signal for blend M50. A sharp increase in the scattered light is observed at 192.0 ± 2.5 °C for M50 (Figure 11). The data for blend M40 are similar to the data for blend M50 and are not shown. The transition temperature determined by SALS for M40 was 180.0 ± 2.5 °C. For both samples, the onset of macrophase separation determined by SALS is in quantitative agreement with that determined by SANS.

In Figure 12, we show the calculated normalized free energy densities of a lamellar phase, a homogeneous phase, and two coexisting macrophases for M50 as a function of temperature. The lamellar-phase free energy is obtained by SCFT, whereas that of the coexisting macrophases is obtained by using Flory−

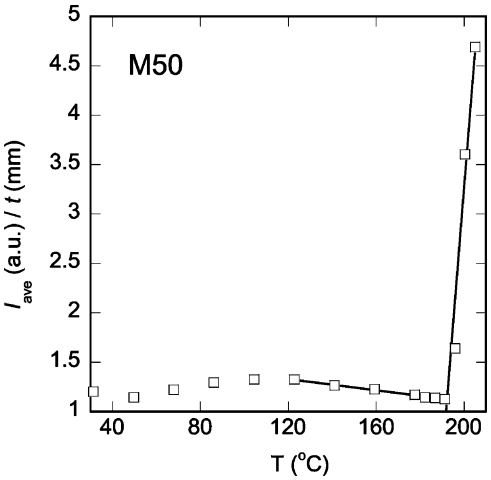

Figure 11. Average SALS intensity (normalized by the sample thickness) as a function of temperature for blend M50. The solid lines in the figure represent a least-squares fit to the data, and the transition temperature is taken to be the intersection of these two lines.

Huggins theory (eq 3) for each of the coexisting phases. For the macrophase-separated state, the total free energy f ($f = f_1\theta_1 + f_2\theta_2$, where θ_1 and θ_2 are the fractions of the system that are in phases 1 and 2, respectively, and f_1 and f_2 are the free energies of phases 1 and 2, respectively) was minimized by changing the values of θ_1, ϕ_{A1}, and ϕ_{B1} (where the latter are the volume fractions of components A and B in phase 1, respectively). The free energy of the homogeneous phase is given directly by eq 3. At low temperatures (30−120 °C), the one-dimensional microphase-separated phase clearly has the lowest free energy. As the temperature approaches 130 °C, the homogeneous macrophase-separated and microphase-separated states have very similar free energies. This might have caused the numerical convergence problems described above. It is clear from the inset, however, that, in the 130−200 °C temperature range, the homogeneous phase has a lower free energy than the macrophase-separated state, whereas at temperatures ≥210 °C, the macrophase-separated state has the lower free energy. The theoretical prediction for the homogeneous-to-macrophase separation transition is thus 205 ± 5 °C.

In Table 5, we summarize our findings by reporting the temperatures of the different phase transitions that we have identified. The first entry in that table compares the theoretically

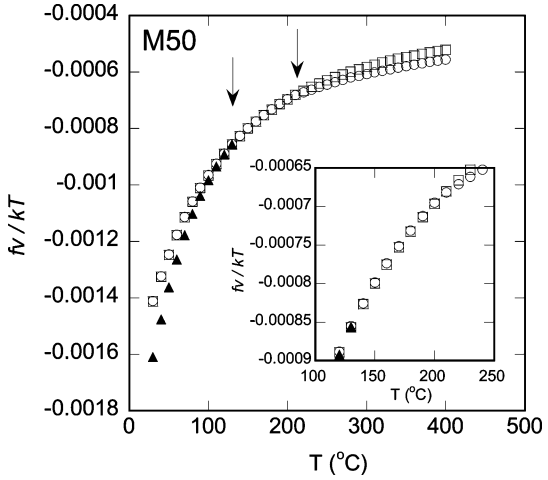

Figure 12. Dimensionless free energy as a function of temperature for M50 for the lamellar phase (▲) as predicted by SCFT and the homogeneous (□) and macrophase-separated (○) phases as predicted by FHT. The arrows indicate phase transitions. Inset: plot of the region of the dimensionless free energy as a function of temperature in which the free energies of the various phases are similar.

Table 5. Phase Transition Temperatures (°C) in Multicomponent Blends[a]

	homogeneous → macrophase-separated		microphase-separated → homogeneous	lamellar → microemulsion
blend	FHT	SALS	RPA/SANS	SANS
M50	205 ± 5	192 ± 2.5	141 ± 10	80 ± 10
M40	165 ± 5	180 ± 2.5	160 ± 10	80 ± 10

[a] FHT is Flory−Huggins theory, RPA is the random-phase approximation, SANS is small-angle neutron scattering, and SALS is small-angle light scattering.

predicted homogeneous-to-macrophase separation transition with experimental measurements for M50. The agreement is almost within experimental uncertainty. The value of the microphase-separated-to-homogeneous transition temperature reported in Table 5 is assumed to be the low-temperature limit of applicability of the RPA. Although the quantitative agreement between RPA predictions and the experimental results give us some confidence in this estimate, we were unable to find any obvious experimental signatures of a discontinuous phase transition from a fluctuating homogeneous phase to a microphase-separated phase. This appears to be a weakly first-order or second-order phase transition. The last M50 entry in Table 5 shows the experimentally determined lamellar-to-microemulsion phase transition. Our theoretical framework does not distinguish between these phases.

We repeated the above analysis for M40 and obtained similar results: microphase separation at low temperatures, a homogeneous phase at intermediate temperatures, and macrophase separation at high temperatures. The numerical values for the transition temperatures are given in Table 5. It is clear that the theoretically computed RPA scattering profiles at high temperatures (≥170 °C in Figure 3 and ≥210 °C in Figure 4) correspond to metastable homogeneous systems. It is interesting to note that M40 has an underlying spinodal (Figure 3), whereas M50 does not (Figure 4).

Conclusions

The thermodynamics and phase behavior of A/B/A−C polymer blends with repulsive A/B and A/C interactions and attractive B/C interactions were studied by a combination of theory and experiment. All of the theoretical predictions were made using independently determined binary Flory−Huggins interaction parameters and statistical segment lengths. Both experiments and theory indicated a series of phase transitions from microphase separation to a homogeneous phase and from a homogeneous phase to a macrophase-separated state with increasing temperature. There is reasonable agreement between the phase transition temperatures obtained by theory and experiment. The sizes of the microphases measured experimentally were in excellent agreement with SCFT-based predictions over the entire temperature window. The scattering profiles measured in the homogeneous state were in quantitative agreement with RPA-based theoretical predictions. It is unusual for microphase-separated polymer blends to become homogeneous prior to macrophase separation. The fact that such complex behavior can be captured by SCFT, FHT, and RPA is an indication of the power of these theoretical constructs.

Acknowledgment. This material is based on work supported by the National Science Foundation under Grant 0305711 and a National Science Foundation Graduate Research Fellowship. The facilities at NIST are supported in part by the National Science Foundation under Agreement DMR-9986442.

References and Notes

(1) Bates, F. S.; Maurer, W.; Lodge, T. P.; Schulz, M. F.; Matsen, M. W.; Almdal, K.; Mortensen, K. *Phys. Rev. Lett.* **1995**, *75*, 4429−4432.
(2) Hillmyer, M. A.; Maurer, W. W.; Lodge, T. P.; Bates, F. S.; Almdal, K. *J. Phys. Chem. B* **1999**, *103*, 4814−4824.
(3) Bates, F. S.; Maurer, W. W.; Lipic, P. M.; Hillmyer, M. A.; Almdal, K.; Mortensen, K.; Fredrickson, G. H.; Lodge, T. P. *Phys. Rev. Lett.* **1997**, *79*, 849−852.
(4) Washburn, N. R.; Lodge, T. P.; Bates, F. S. *J. Phys. Chem. B* **2000**, *104*, 6987−6997.
(5) Morkved, T. L.; Chapman, B. R.; Bates, F. S.; Lodge, T. P.; Stepanek, P.; Almdal, K. *Faraday Discuss.* **1999**, 335−350.
(6) Cohen, R. E.; Ramos, A. R. *Macromolecules* **1979**, *12*, 131−134.
(7) Datta, S.; Lohse, D. J. *Polymeric Compatibilizers*; Hanser: Cincinnati, OH, 1996.
(8) Hudson, S. D.; Jamieson, A. M. In *Polymer Blends*; Paul, C. B., Ed.; Wiley: New York, 2000; Vol. 1.
(9) Jeon, H. S.; Lee, J. H.; Balsara, N. P. *Phys. Rev. Lett.* **1997**, *79*, 3274−3277.
(10) Jeon, H. S.; Lee, J. H.; Balsara, N. P. *Macromolecules* **1998**, *31*, 3328−3339.
(11) Jeon, H. S.; Lee, J. H.; Balsara, N. P.; Newstein, M. C. *Macromolecules* **1998**, *31*, 3340−3352.
(12) Lyu, S.; Jones, T. D.; Bates, F. S.; Macosko, C. W. *Macromolecules* **2002**, *35*, 7845−7855.
(13) Tan, N. C. B.; Tai, S. K.; Briber, R. M. *Polymer* **1996**, *37*, 3509−3519.
(14) Jackson, C. L.; Sung, L.; Han, C. C. *Polym. Eng. Sci.* **1997**, *37*, 1449−1458.
(15) Sung, L.; Hess, D. B.; Jackson, C. L.; Han, C. C. *J. Polym. Res. (Taiwan)* **1996**, *3*, 139.
(16) Koizumi, S.; Hasegawa, H.; Hashimoto, T. *Macromolecules* **1994**, *27*, 7893−7906.
(17) Kielhorn, L.; Muthukumar, M. *J. Chem. Phys.* **1997**, *107*, 5588−5608.
(18) Balsara, N. P.; Jonnalagadda, S. V.; Lin, C. C.; Han, C. C.; Krishnamoorti, R. *J. Chem. Phys.* **1993**, *99*, 10011−10020.
(19) Leibler, L. *Makromol. Chem., Macromol. Symp.* **1988**, *16*, 1−17.
(20) Leibler, L. *Physica A* **1991**, *172*, 258−268.
(21) Broseta, D.; Fredrickson, G. H. *J. Chem. Phys.* **1990**, *93*, 2927−2938.
(22) Mathur, D.; Hariharan, R.; Neuman, E. B. *Polymer* **1999**, *40*, 6077−6087.
(23) Wang, Z. G.; Safran, S. A. *J. Phys.* **1990**, *51*, 185−200.
(24) Janert, P. K.; Schick, M. *Macromolecules* **1997**, *30*, 3916−3920.
(25) Janert, P. K.; Schick, M. *Macromolecules* **1997**, *30*, 137−144.
(26) Muller, M.; Schick, M. *J. Chem. Phys.* **1996**, *105*, 8885−8901.
(27) Maric, M.; Macosko, C. W. *J. Polym. Sci. B: Polym. Phys.* **2002**, *40*, 346−357.
(28) Schnell, R.; Stamm, M.; Rauch, F. *Macromol. Chem. Phys.* **1999**, *200*, 1806−1812.
(29) Zhao, H. Y.; Huang, B. T. *J. Polym. Sci. B: Polym. Phys.* **1998**, *36*, 85−93.

(30) Ruzette, A. V.; Leibler, L. *Nat. Mater.* **2005**, *4*, 19−31.
(31) Tanaka, H.; Hasegawa, H.; Hashimoto, T. *Macromolecules* **1991**, *24*, 240−251.
(32) Lee, J. H.; Balsara, N. P.; Krishnamoorti, R.; Jeon, H. S.; Hammouda, B. *Macromolecules* **2001**, *34*, 6557−6560.
(33) Lee, J. H.; Ruegg, M. L.; Balsara, N. P.; Zhu, Y. Q.; Gido, S. P.; Krishnamoorti, R.; Kim, M. H. *Macromolecules* **2003**, *36*, 6537−6548.
(34) Reynolds, B. J.; Ruegg, M. L.; Balsara, N. P.; Radke, C. J.; Shaffer, T. D.; Lin, M. Y.; Shull, K. R.; Lohse, D. J. *Macromolecules* **2004**, *37*, 7401−7417.
(35) Xu, Z.; Jandt, K. D.; Kramer, E. J.; Edgecombe, B. D.; Fréchet, J. M. *J. Polym. Sci. B: Polym. Phys.* **1995**, *33*, 2351−2537.
(36) Shull, K. R.; Kellock, A. J.; Deline, V. R.; MacDonald, S. A. *J. Chem. Phys.* **1992**, *97*, 2095−2104.
(37) Adedeji, A.; Hudson, S. D.; Jamieson, A. M. *Macromolecules* **1996**, *29*, 2449−2456.
(38) Adedeji, A.; Lyu, S.; Macosko, C. W. *Macromolecules* **2001**, *34*, 8663−8668.
(39) Chun, S. B.; Han, C. D. *Macromolecules* **2000**, *33*, 3409−3424.
(40) Auschra, C.; Stadler, R.; Voigt-Martin, I. G. *Polymer* **1993**, *34*, 2081−2093.
(41) Auschra, C.; Stadler, R.; Voigt-Martin, I. G. *Polymer* **1993**, *34*, 2094−2110.
(42) Kahlweit, M.; Strey, R. *Angew. Chem., Int. Ed. Engl.* **1985**, *24*, 654−668.
(43) Kahlweit, M.; Strey, R.; Firman, P.; Haase, D. *Langmuir* **1985**, *1*, 281−288.
(44) Kahlweit, M.; Strey, R.; Haase, D.; Firman, P. *Langmuir* **1988**, *4*, 785−790.
(45) Strey, R. *Colloid Polym. Sci.* **1994**, *272*, 1005−1019.
(46) Chen, S. H.; Choi, S. *Supramol. Sci.* **1998**, *5*, 197−206.
(47) Magid, L.; Butler, P.; Payne, K.; Strey, R. *J. Appl. Crystallogr.* **1988**, *21*, 832−834.
(48) Lin, C. C.; Jeon, H. S.; Balsara, N. P.; Hammouda, B. *J. Chem. Phys.* **1995**, *103*, 1957−1971.
(49) de la Cruz, M. O.; Sanchez, I. C. *Macromolecules* **1986**, *19*, 2501−2508.
(50) Kline, S. NIST Center for Neutron Research, National Institute of Standards and Technology, Gaithersburg, MD, 2001. Unpublished results.
(51) Balsara, N. P.; Lohse, D. J.; Graessley, W. W.; Krishnamoorti, R. *J. Chem. Phys.* **1994**, *100*, 3905−3910.
(52) Lee, J. H. Ph.D. Thesis in Chemical Engineering, University of California at Berkeley, Berkeley, CA, 2002; p 151.
(53) Benoit, H.; Benmouna, M.; Wu, W. L. *Macromolecules* **1990**, *23*, 1511−1517.
(54) Akcasu, A. Z.; Tombakoglu, M. *Macromolecules* **1990**, *23*, 607−612.
(55) de Gennes, P. G. *Scaling Concepts in Polymer Physics*; Cornell University Press: Ithaca, NY, 1979.
(56) Helfand, E. *J. Chem. Phys.* **1975**, *62*, 999−1005.
(57) Evers, O. A.; Scheutjens, J.; Fleer, G. J. *Macromolecules* **1990**, *23*, 5221−5233.
(58) Matsen, M. W. *J. Phys.-Condens. Matter* **2002**, *14*, R21−R47.
(59) Thompson, R. B.; Matsen, M. W. *J. Chem. Phys.* **2000**, *112*, 6863−6872.
(60) Shull, K. R.; Kramer, E. J. *Macromolecules* **1990**, *23*, 4769−4779.
(61) Duchs, D.; Schmid, F. *J. Chem. Phys.* **2004**, *121*, 2798−2805.
(62) Jinnai, H.; Hasegawa, H.; Hashimoto, T.; Han, C. C. *J. Chem. Phys.* **1993**, *99*, 4845−4854.
(63) The relative intensities of the primary and second-order peaks expected from M50b can be estimated by SCFT calculations, as described in ref 34. These calculations indicate that the expected scattering intensities from the primary and secondary peaks in M50 would be lower than those obtained from the sample studied in ref 34 by multiplicative factors of 0.13 and 0.30, respectively. It is thus not entirely surprising that the SANS profiles obtained from M50b were devoid of peaks.
(64) Brazovskii, S. A. *Sov. Phys.−JETP* **1975**, *41*, 85−89.
(65) Fredrickson, G. H.; Helfand, E. *J. Chem. Phys.* **1987**, *87*, 697−705.
(66) Duchs, D.; Ganesan, V.; Fredrickson, G. H.; Schmid, F. *Macromolecules* **2003**, *36*, 9237−9248.

MA0516889